Identification of Alcohol Dehydration Sites on an Oxide Surface by Scanning Tunneling Microscopy

ARTICLE *in* THE JOURNAL OF PHYSICAL CHEMISTRY B · NOVEMBER 2000

Impact Factor: 3.3 · DOI: 10.1021/jp003217o

Identification of Alcohol Dehydration Sites on an Oxide Surface by Scanning Tunneling Microscopy

Robert E. Tanner,* Pornthep Meethunkij, and Eric I. Altman

Department of Chemical Engineering, Yale University, P.O. Box 208286, New Haven, Connecticut 06520-8286

Received: September 13, 2000

High-speed scanning tunneling microscopy (STM), temperature-programmed desorption (TPD), Auger electron spectroscopy and low-energy electron diffraction (LEED) were used to characterize the (001) surface of monoclinic γ-WO_3, and to determine the structure and reactivity of active sites on this surface. Cleavage along the WO_3(001) plane followed by heating in O_2 to remove carbonaceous impurities and subsequent reduction above 775 K in $\sim 10^{-5}$ Torr of O_2 resulted in a c(2×2) reconstruction that is visible in LEED and atomic resolution STM images. The catalytic activity of the c(2×2) surface was probed through exposure to a series of alcohols. No difference in the sticking coefficient for 1-propanol, 2-propanol and 2-methyl-2-propanol (*tert*-butyl alcohol) was detectable. As the surface temperature was increased during TPD, desorption of unreacted alcohol and water was seen at temperatures less than 600 K, independent of the alcohol. The water desorption is attributed to deprotonation of the adsorbed alcohols to form alkoxides; at this stage STM images show terraces covered with adsorbates with no preference for the adsorbates to occupy step or other defect sites. At higher temperatures the alkoxide all desorbs as alkenes: no dehydrogenation products were observed, indicating that the c(2×2) surface displays only dehydration activity under these conditions. The alkene desorption peak temperature decreases from primary to tertiary alcohol (1-propanol → *tert*-butyl alcohol), indicating that desorption is limited by the rate of C−O bond scission of the adsorbed alkoxide. STM images are presented in which the alkoxide intermediates are resolved simultaneously with atomic resolution of the WO_3(001)-c(2×2) substrate. These demonstrate that the sites for oxidative dehydration of the alcohol molecules are the exposed 5-fold coordinated W^{6+} ions. Further, it is demonstrated that the alkoxide can be removed from the surface with the STM tip to reveal the structure of the underlying adsorption sites.

I. Introduction

Transition metal oxides find applications in many different areas of heterogeneous catalysis, both as supports and for their own catalytic properties. Some are employed for their photocatalytic properties, while others are used in a wide range of reactions, including partial oxidation reactions and the selective reduction of NO. Among catalytically active transition metal oxides (TMO), tungsten trioxide is noteworthy as it also exhibits ferroelectric, electrooptic and semiconducting properties, and tungsten bronzes are formed upon incorporation of metals, ammonium ions and hydrogen into the lattice. Tungsten trioxide also displays color centers upon irradiation with ultraviolet light, doping with high-mobility protons or application of an electrical field.[1] The surface properties of WO_3 are exploited in applications such as gas sensors[2] and thin-film electrochromic displays,[3,4] where donor atoms are added to the dodecahedral interstices of the oxygen sublattice to give the film its desired color. Supported tungsten oxide is known to be catalytically active for alcohol dehydrogenation, alkane hydrogenation and metathesis,[5] and is attracting attention for the solid-acid properties that can be exploited in acid-catalyzed reactions such as the hydroisomerization of alkanes.[6−10] Despite these diverse applications, the relationship between catalytic activity or function (e.g., dehydrogenation versus dehydration of alcohols) and catalyst structure remains a subject of debate both for TMOs in general and for WO_3 specifically. At the surface of many oxides, coordinatively unsaturated sites (cus) have been identified as active centers for catalysis.[11] It is well accepted that the catalytic activity of these sites can depend on the oxidation state of the cus metal cation. Furthermore, the catalytic activity and function of TMOs can also be structure-sensitive. Some have suggested that structure sensitivity is related to the different catalytic properties of neighboring bridging and terminal oxygen species, while others have argued that terminal oxygen is irrelevant to catalysis.[12,13] This has motivated us to study the effects of cation oxidation state and terminal oxygen concentration on oxide catalysis. On the surface of monoclinic γ-WO_3(001) these two parameters can be varied systematically, and in this paper we identify the alcohol dehydration sites using scanning tunneling microscopy (STM) and temperature-programmed desorption (TPD).

Bulk WO_3 exhibits a perovskite-like structure. Between 100 and 1000 K it displays a series of polymorphs, based on an idealized cubic ReO_3 corner-sharing, octahedral network. The five observed phases are deviations from the ideal structure due to two distorting effects: displacement of the tungsten atoms from the center of their octahedra, and tilting of the WO_6 octahedra. As it is cooled from its melting temperature, the symmetry of WO_3 changes from tetragonal to a second tetragonal phase, to orthorhombic, to monoclinic at room temperature. Further cooling changes the symmetry to triclinic and finally a second monoclinic form.[14−16] The room-temperature phase, γ-WO_3, is monoclinic, space group $P2_1/n$ (C_{2h}^5). Its unit cell is a distorted $2 \times 2 \times 2$ arrangement of ideal ReO_3-type units, since the W−O−W bond angle is alternately greater

* Address correspondence to this author. Fax: +1 203 432-4387. E-mail: robert.tanner@yale.edu. URL: http://www.eng.yale.edu/.

10.1021/jp003217o CCC: $19.00
Published on Web 12/01/2000

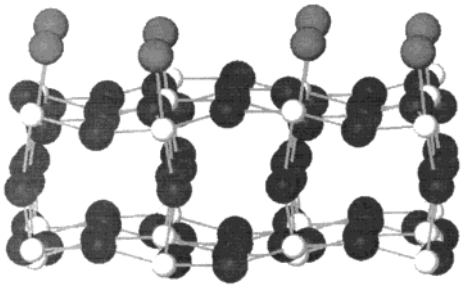

Figure 1. Model for γ-WO_3, highlighting the monoclinic distortion of the idealized cubic ReO_3 structure. Small, light spheres represent tungsten cations; the large, dark spheres bridging oxygen anions; and the large, light gray spheres terminal oxygen anions. Atoms are in their unrelaxed positions.

than and less than 180° along each of the three principal axes, as seen in Figure 1. The lattice parameters[17] for this phase are $a_0 = 7.297$ Å, $b_0 = 7.539$ Å, $c_0 = 7.688$ Å, $\beta = 90.91°$ and it is stable between 290 and 603 K. Oxygen deficiency reduces the temperature of the transition to the triclinic phase upon cooling, and the change to orthorhombic symmetry upon heating appears to take place over a range of about 100 K, being complete at around 740 K.[1,18] Such oxygen deficiency also increases the bulk electronic transport properties of WO_3, which has a band gap of 2.6 eV in its stoichiometric form.[19] The creation of oxygen deficiency and substoichiometric WO_{3-x} is accompanied by the appearance of electronic donor states in the band gap due to cation reduction. Further reduction leads to crystallographic shear (CS) plane formation during which edge-sharing octahedra are created. The lattice collapses to eliminate ordered planes of oxygen vacancies, particularly if the reduced sample is ground before analysis.[20]

Recent studies suggest that the (001) surface of γ-WO_3 is ideal for studying the effect of cation reduction and bridging versus terminal oxygen on the catalytic properties of TMOs. Detailed STM, low-energy electron diffraction (LEED) and photoelectron spectroscopy (PES) studies of the γ-WO_3(001) surface have confirmed the theoretical model, in which a surface dipole is avoided[21] by covering the topmost WO_2 plane by half a monolayer (ML) of terminal oxygen (Figure 2).[22−25] This c(2 × 2) surface exposes W^{6+} ions surrounded by bridging and terminal oxygen. Removal of further terminal oxygen from the autocompensated c(2 × 2) surface is accompanied by reduction of the formal charge on the tungsten atoms to W^{5+}.[21] Via this process, p(2 × 2) and (1 × 1) reconstructions may be created and STM observations have revealed both structures.[23−25] Thus, studying the chemical properties of γ-WO_3(001) as the surface is reduced from c(2 × 2) to (2 × 2) to (1 × 1) offers the opportunity both to characterize the effect of cation reduction while maintaining both bridging and terminal oxygen, and to determine the effect of terminal oxygen on the catalytic activity and function of reduced cations. Though the valence electrons on reduced W^{5+} ions are localized in 5*d* atomic orbitals that point outward from the surface, and thus are expected to be chemically very active,[26−31] there has been little work on determining the chemical properties of well-characterized WO_3 surfaces.[32−35]

Against this background, we have begun to characterize the surface chemistry of γ-WO_3(001) systematically as the surface is reduced, principally using TPD and STM. The TPD measurements are directed toward determining the surface's relative activity for oxidative dehydrogenation versus dehydration by characterizing adsorption−desorption kinetics and desorption products for a series of alcohols that are progressively easier to

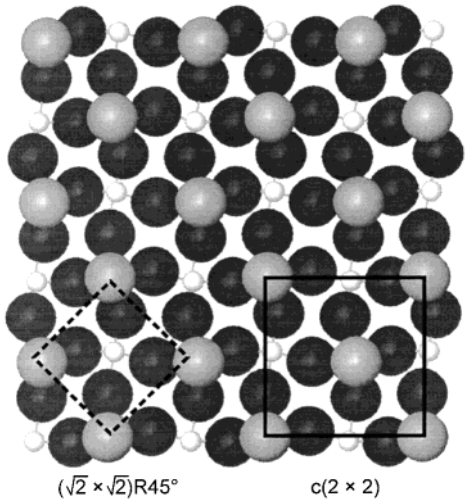

Figure 2. Model for the top two layers of γ-WO_3(001), showing the c(2 × 2) reconstruction. The squares highlight the two equivalent descriptions of the surface unit cell: c(2 × 2) (solid) and ($\sqrt{2}$ × $\sqrt{2}$)R45° (dashed). Small, light spheres represent tungsten cations; the large, dark spheres bridging oxygen anions; and the large, light gray spheres terminal oxygen anions. All atoms are in their unrelaxed positions.

dehydrate. The STM experiments have two major goals: the first is to relate features in the desorption traces to specific surface phases; the second goal is to determine the active site directly by imaging the reactive intermediates − particularly important for oxides since defects such as steps and vacancies can dominate the adsorption properties of oxides.

This paper focuses on the surface chemistry of the c(2 × 2) surface. It will be shown that the c(2 × 2) surface exhibits only dehydration activity, that the rate-limiting step in alcohol dehydration to alkenes is C−O bond scission, that the alkoxide intermediate bonds to exposed W^{6+} ions on the terraces, that the alkoxide displays no enhanced affinity for steps or other defects over terrace sites, and that the adsorbed intermediates can be removed from the surface with the STM tip thus revealing the structure of the underlying substrate.

II. Experimental Section

a. Experimental Apparatus. Experiments were carried out using an ultrahigh vacuum (UHV) chamber equipped with low-energy electron diffraction optics, a double-pass cylindrical mirror analyzer for Auger electron spectroscopy (AES) and low-energy ion scattering spectroscopy (LEISS), a sputter-ion gun, a quadrupole mass spectrometer (QMS) with capabilities for TPD and temperature-programmed mass spectrometry (TPMS), as well as the scanning tunneling microscope. The microscope is capable of collecting images at rates in excess of 1 frame/s and at temperatures ranging between 300 and 1000 K; further details of the design of the instrument are given elsewhere.[36] A 300 ls^{-1} ion pump in the system's main chamber provided a base pressure better than 1×10^{-10} Torr, while a backed turbomolecular pump was used to remove sputter gases and evacuate a preparation chamber that can be valved-off from the main chamber. In the preparation chamber, samples can be heated to temperatures in excess of 800 K at pressures up to 10 Torr.

Various sources and dosers within the chamber allow real-time STM monitoring of in-situ deposition, adsorption, and reaction. For this study, the chamber was configured with two leak valves fitted to directed dosers; one aimed at the tunnel junction of the STM for in-situ reaction and adsorption studies,

the second aimed at the sample manipulator for TPD and LEED studies. Previously, it was shown that positioning the sample in front of the manipulator doser results in an effective pressure 45 times greater than the background pressure while the STM doser gives an enhancement of a factor of 5.[37] The slow pumping speed of the alcohols, however, makes these numbers only approximate for this study.

b. Tip and Sample Preparation. Dark green WO_3 crystals were grown in a $NaF-PbF_2$ flux at the Clarendon Laboratories in Oxford.[38] They were stored in air, and cleaved to expose a (001) surface prior to insertion into the vacuum chamber. The antiferroelectric distortion of the W-sublattice in the WO_3 crystals causes a layering of the structure along the [001] crystallographic direction, and so cleavage is facile and the surface is stable. The crystals were secured to a Ta backing plate at top and bottom with Pt−Ir wire, and the plate was clamped to a Mo holder using ceramic strips of low-thermal-expansion Aremcolox 502-1550. The temperature was measured using a chromel−alumel thermocouple spot-welded to one of the Pt−Ir securing wires. The sample was heated in the preparation chamber using an infrared lamp located outside the UHV system. By focusing the light onto the sample through a quartz window, the samples could easily be heated to temperatures in excess of 900 K. In the main chamber, the crystals were heated via conduction from the Ta backing plate, which in turn was heated via conduction from two resistively heated Ta wires. Further details of the sample holder design can be found in ref 36.

Once inserted into the vacuum chamber, impurities were removed by annealing in $\sim 10^{-5}$ Torr of O_2 at 775−885 K. After several hours, AES showed peaks due to only W and O.

Tips were prepared from 0.25 mm diameter polycrystalline W wire by electrochemical etching in NaOH solution. After washing in methanol they were directly inserted into the preparation chamber. Electron-beam bombardment of the tips prior to use ensured that any contaminants were desorbed from the tungsten surface.

c. Experimental Procedure. Alcohols for these experiments were purified using freeze−pump−thaw cycles until the line pressure did not rise above background (5×10^{-4} Torr). They were supplied to the chamber through either of the two leak valves on the main chamber. Dosing was performed at room temperature. As described in section III, TPMS experiments were performed following alcohol exposure in which full range mass spectra were repeatedly obtained while the sample temperature was ramped. This procedure identified the masses of the cracking fragments to be monitored in subsequent TPD experiments. During the TPD experiments, up to six masses were monitored. Where two or more fragments from the same molecule were monitored, the TPD curves presented in this paper are the sum of those two traces, increasing the signal-to-noise ratio. A heating rate of 5 K s^{-1} was used, and the experiments were performed with the sample in line-of-sight of the ionizer of the quadrupole mass spectrometer.

To determine the contribution of alcohol adsorption on the sample holder to the TPD results, mica samples were mounted in the same manner and subjected to the same cleaning procedure as the WO_3 crystals and then exposed to the alcohols. These mica samples displayed no measurable desorption of alcohols, alkenes, and water in the temperature regime where these species were observed to desorb from the WO_3 crystals.

Scanning tunneling microscopy images were acquired at room temperature in constant current mode at tunneling currents between 0.1 and 1.0 nA and positive sample bias only (i.e., empty-states imaging). Images of the highest quality were obtained at high biases (typically 1.5−3.0 V), though imaging of the clean surface was also possible at lower biases. We were not able to achieve stable tunneling from filled valence band states. This behavior is expected, since substoichiometric WO_{3-x} is an n-type semiconductor in which donor states in the band gap, created through oxygen deficiency, pin the Fermi level to the bottom of the conduction band.[25,33,35] We attribute the inability to image at negative sample biases to the prohibitively large band gap of 2.6 eV. For the adsorbate-covered surfaces, it was found that imaging at biases less than 2.0−2.5 V significantly disrupted the surface.

III. Results and Discussion

a. WO_3(001) Surface Structure and the Effect of Surface Treatment. It was found that the surface structure could be manipulated by varying the preparation conditions. Heating in an oxygen pressure above 10^{-5} Torr at 775−885 K to remove carbonaceous impurities resulted in a poor quality c(2 × 2) LEED pattern. Reducing the oxygen pressure during annealing caused the c(2 × 2) LEED pattern to become progressively sharper with time, while the diffuse background decreased (Figure 3a). The splitting of the spots has previously been attributed to twinning of the crystal to form domains with the monoclinic tilt rotated by 90°, 180° and 270°.[22,32] Simultaneously with the evolution of the c(2 × 2) pattern, STM images revealed the formation of c(2 × 2) domains. Figures 3b,c and 4 show STM images obtained after annealing for more than 10 h in 3×10^{-5} Torr of O_2 at temperatures between 775 and 800 K. Monatomic steps are visible in Figure 3b, and the high-resolution image of the same area (Figure 3c) reveals a square lattice. The repeat distance between the bright features is 5.2 Å, or $\sqrt{2}$ times the 3.7 Å lattice constant of idealized cubic WO_3, consistent with a c(2 × 2) structure. From linescans across the image, we determine the apparent height of the bright features to be 0.75 Å above the occasional dark patches (where bright features are missing). In Figure 4, two images extracted from an STM movie are presented. Figure 4a shows a terrace where the bright features are again arranged with c(2 × 2) periodicity. The periodicity is broken by individual missing bright features, and by denuded areas (marked "D") where several features are absent. The image recorded 2.5 s later shows that some of the bright spots have become dim, while some dim areas have become bright; the stars highlight the positions where the surface has changed. The movie demonstrates that motion on the oxide surface is rapid, even at room temperature.

In the model for the WO_3(001)-c(2 × 2) reconstruction shown in Figure 2, the surface terminates with half a monolayer (ML) of oxygen atoms (larger, light gray spheres). If both O and W maintain their formal charge of 2− and 6+, this reconstruction yields a neutral surface with zero net surface dipole. Consistent with this model, previous PES studies suggest that the c(2 × 2) surface is fully oxidized.[25] On this basis, and in view of the periodicity in Figures 3c and 4, we assign the bright features to terminal oxygen atoms. Image formation in the STM is dominated by two major mechanisms: topographic contrast and electronic contrast. In the former mode, bright features correspond to positions where the tip retracts to maintain a constant tunneling current as it surmounts protuberances from the surface. Bright features due to electronic contrast reflect tip retraction where the electron density contour bulges outward from the surface. On oxide surfaces both contrast mechanisms can contribute to the image.[39] Simulations show a relaxation of the terminal W−O bond length to 1.6 Å.[31] At the same time,

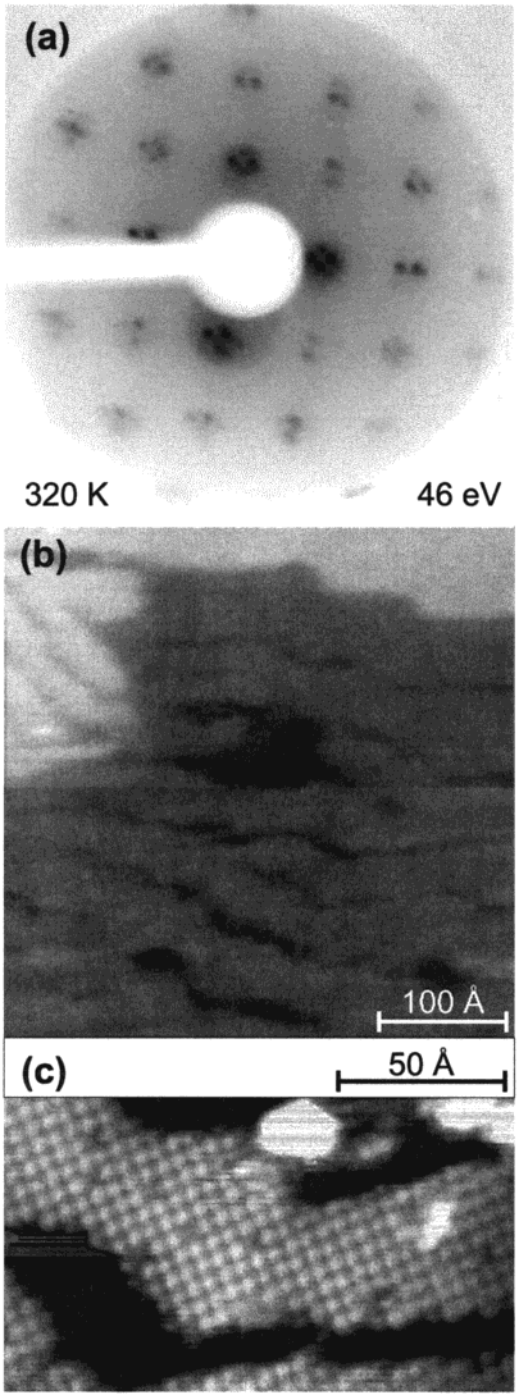

Figure 3. $WO_3(001)$ surface after heat treatment ~1 h in 3×10^{-5} Torr of O_2 at 790 K. (a) A contrast-reversed low-energy electron diffraction of the room-temperature monoclinic phase (space group $P2_1/n$). The splitting of the spots has been attributed to twinning of monoclinic microdomains along the [010] direction. (b) STM constant current topograph of the surface, showing a step and line-defects. Imaging conditions $V_B = 2.0$ V, $I_t = 0.55$ nA. (c) High-resolution image of the surface shown in (b), revealing atomic periodicity that confirms the c(2 × 2) pattern observed in LEED. $V_B = 2.75$ V, $I_t = 0.55$ nA.

the unoccupied states are concentrated at the W atoms, with some covalency 2 eV above the Fermi level leading to unoccupied state density at the O atoms. In this case the height difference between the W and O atoms dominates the difference in electronic density, and the terminal oxygen appears raised, i.e., the bright points correspond to protruding oxygen atoms.[23,31]

The movement of the bright features in the STM movie

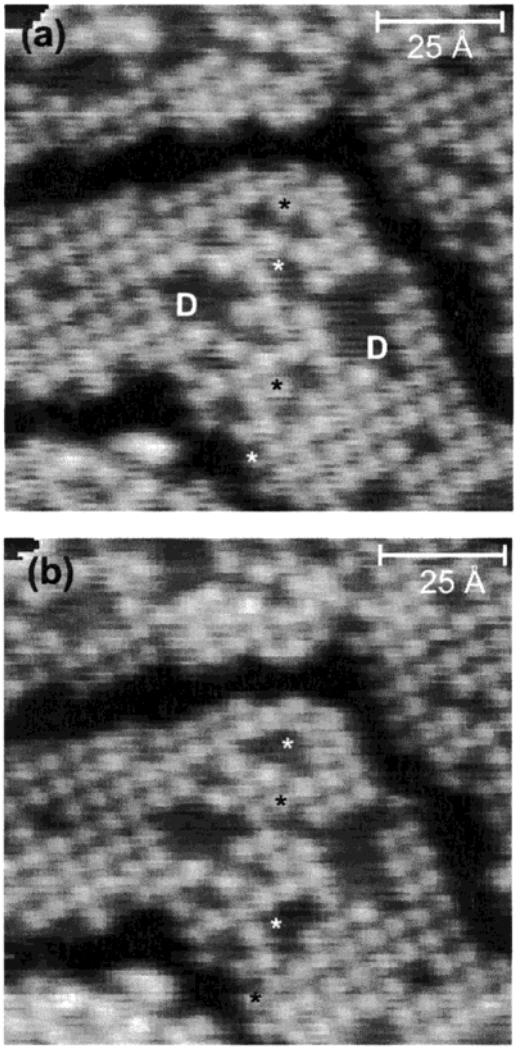

Figure 4. Two images, recorded 2.5 s apart, from a movie of the $WO_3(001)$-c(2 × 2) surface. Positions where the terminal oxygen atoms and vacancies are not present in the other image are indicated by black and white stars, respectively. Larger denuded areas are marked with a "D". $V_B = 1.25$ V, $I_t = 0.55$ nA.

(Figure 4) confirm this picture. Since the W atoms in the WO_2 plane are coordinated to at least five oxygen atoms, W atom diffusion is considered unlikely and thus the changes are attributed to diffusion of singly coordinated terminal oxygen atoms. It could still be argued that the W atoms are imaged and that terminal oxygen causes the underlying W atom to appear dimmer than exposed W atoms. This, however, would suggest that the bare patches at the center of Figure 4a,b are completely covered by terminal oxygen, which would require W atoms in an unphysical "7+ oxidation state". Therefore, the bare patches are associated with areas where all the terminal oxygen has been removed. As expected, the measured depth of the bare patches is less than the relaxed surface W−O bond length[30] (0.75 Å versus 1.6 Å). The difference between the actual height and the height measured with STM reflects the lower integrated local density of states (LDOS) at the oxygen atoms. For typical values of the tunneling barrier height, the 0.95 Å difference between the measured and actual height indicates roughly an order of magnitude difference in the DOS between the terminal O atom and the bare patches.

Although heating in 3×10^{-5} Torr of O_2 results in the formation of well-ordered c(2 × 2) terraces, the densities of certain types of defects were observed to increase as the

c(2 × 2) domains spread across the surface. Three types of surface defects were visible in STM images. The initial effect is an increase in the density of monatomic steps and continued annealing produced the dark defect lines running through the terraces parallel to the WO_3 [100] and [010] directions (Figure 3b). A third defect-type, dark point defects, is seen in the atomic-resolution image in Figure 3c. Again, since the c(2 × 2) arrangement of bright spots is due to the terminal oxygen, the dark point defects are attributed to oxygen vacancies. The dark lines in Figure 3b have previously been attributed to regions where all the terminal oxygen has been removed, possibly in combination with bulk shear planes.[23] The images in Figure 4, however, show that bare patches in which all the terminal oxygen is removed are not as deep as the troughs. Further, in areas where the lines were sufficiently wide to allow imaging of the bottom of the troughs, the images revealed terminal oxygen species and line depths that were multiples of the unit cell height. Images recorded as a function of annealing time at 3×10^{-5} Torr suggest that the lines are boundaries between growing c(2 × 2) terraces.[40] Regardless of the origin of the defects, to an adsorbing molecule the defect boundaries appear indistinguishable from steps.

b. Alcohol Adsorption and Reaction on WO_3(001) via TPD. To gauge the catalytic activity of the WO_3(001) surface, we chose to investigate the oxidative dehydrogenation versus dehydration behavior of the series of alcohols methanol, 1-propanol (*n*-propanol), 2-propanol (2-propanol) and 2-methyl-2-propanol (*tert*-butyl alcohol) using TPD. The dehydration reactions yield alkenes and/or ethers while dehydrogenation yields carbonyls and carboxylates. By comparing the product distribution for the series of alcohols, which are progressively easier to dehydrate, a measure of the surface's relative activity for the two catalytic functions can be obtained. Further, comparison of the desorption peak temperatures provides insight into the reaction mechanism and kinetics. In this paper we focus on the reactivity of the c(2 × 2) surface; we are currently working on determining how the surface chemistry changes when the surface is reduced.

Initially, TPMS experiments were performed to determine the desorption products for fully oxidized WO_3 surfaces exhibiting sharp c(2 × 2) LEED patterns. Full range mass spectra were recorded as the sample temperature was ramped. Following a 1000 L 2-propanol dose at 310 K, desorption in two temperature regimes was observed. Between 380 and 470 K, a weak feature consisting of predominantly mass 45 was observed. Between 575 and 720 K, a much stronger feature with signals at 42, 41, 40, 39, 38, 27, 26, and 15 amu was observed. The product distribution did not change with exposure and no H_2 desorption was observed in TPMS.

Mass 45 corresponds to C_2H_5O, the predominant cracking fragment of 2-propanol, while mass 42 corresponds to C_3H_6 (propene, propylene). All the other features can be assigned to cracking fragments of propene. Thus, it was concluded that 2-propanol adsorption on the c(2 × 2) surface leads to desorption of unreacted alcohol and the dehydration product propene. On the basis of these results, during 2-propanol TPD runs, masses 45 and 58 corresponding to 2-propanol; masses 42, 41, and 39, corresponding to propene; and mass 18 corresponding to water were monitored. These masses were selected to provide the most intense signal, while minimizing overlap between fragments that are common to 2-propanol and propene.

Figure 5 shows a series of TPD curves obtained as a function of 2-propanol exposure. Prior to obtaining these data, STM images were obtained that were similar to those shown in Figures 3 and 4, thus the data reflect exposure to a surface with c(2 × 2) terraces, steps, line defects, and terminal oxygen vacancies. At the lowest coverages, propene desorption is observed in a peak centered at 660 K. As the coverage increases, unreacted 2-propanol desorbs in a broad peak at 430 K, and small amounts of water were observed to desorb simultaneously with the unreacted alcohol and the propene. The ratio of the unreacted alcohol desorbing compared to the amount of propene formed increases with exposure; however, it is difficult to determine the exact branching ratio because of differences in the sensitivity of the mass spectrometer to the different species. The propene desorption peak temperature is observed to shift only slightly with coverage, from 660 K at the lowest coverages to 645 K at saturation. The desorption peaks were observed to saturate after an exposure of ~300 L.

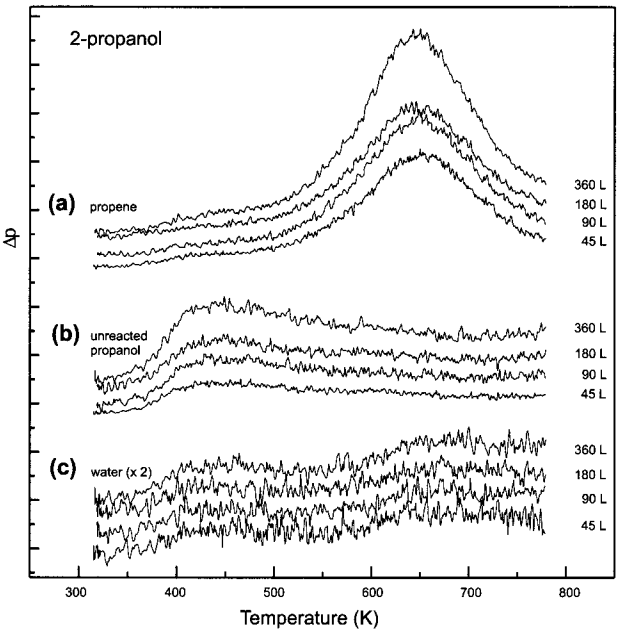

Figure 5. TPD traces as a function of 2-propanol dose on the WO_3(001)-c(2 × 2) surface. The individual traces are offset along the pressure axis for clarity.

The small peak-shift with temperature suggests that propene desorption is first order, as would be expected for a unimolecular reaction, and that the adsorbates only weakly interact with one another. Thus, even at saturation, the propene desorption can be associated with the chemistry of individual sites. Although 2-propanol dehydration yields one water molecule per propene molecule, the water desorption features were surprisingly small, particularly given the low pumping rates expected for water. This could be due to H intercalation into the bulk to form the well-known hydrogen tungsten bronze. Such intercalation has been observed for MoO_3 following reaction with alcohols.[41] Alternatively it could be due to the sensitivity of the QMS to the different species, or the fact that the alcohol and alkene traces are sums of the signals from more than one fragment.

Both 1-propanol and *tert*-butyl alcohol behave similarly to 2-propanol. The TPMS results for 1-propanol showed desorption in two regimes: at lower temperatures predominantly masses 58 (C_3H_6O) and 31 (CH_2OH) which can be associated with 1-propanol were observed; while at higher temperatures masses 42, 41, 40, 39, 38, 27, 26, and 15 amu which are all associated with propene were observed. Thus, again there was no evidence of oxidative dehydrogenation. For 1-propanol TPD experiments, masses 58 and 45 were monitored for 1-propanol desorption along with 18 for water and 42, 41, and 39 amu for propene.

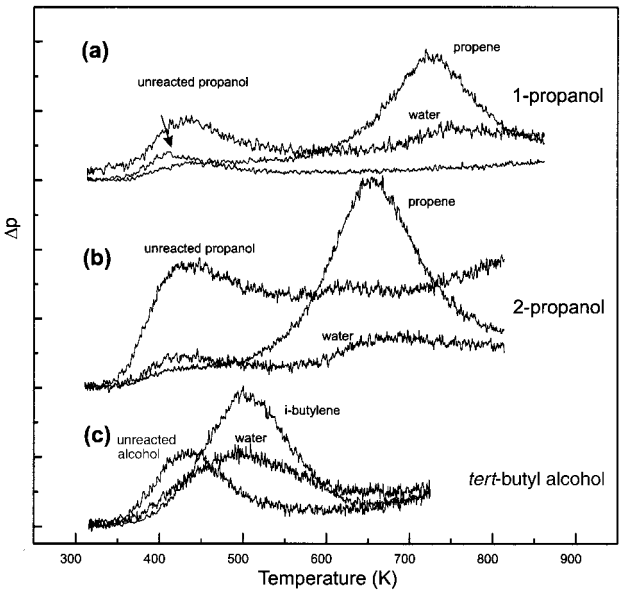

Figure 6. Temperature-programmed desorption traces following dosing of the $WO_3(001)$ surface with different alcohols. The curves presented are selected masses from the cracking patterns of (a) 1-propanol, (b) 2-propanol, and (c) 2-methyl-2-propanol (*tert*-butyl alcohol). A heating rate of 5 K s^{-1} was used for all measurements.

For *tert*-butyl alcohol, at lower temperatures the TPMS showed signals at 59 (C_3H_7O), 41, 28, and 27 amu which can all be associated with *tert*-butyl alcohol, and at higher temperatures masses 56 (C_4H_8), 53, 51, 50, 42, 41, and 39 amu were observed, which can all be associated with isobutene (isobutylene). Again, no oxidative dehydrogenation products were observed. For *tert*-butyl alcohol TPD, mass 59 was monitored for *tert*-butyl alcohol, 18 for water, and 56, 53, 42, and 39 for isobutylene. It was found that roughly the same doses were required to saturate the surface with either 1-propanol, 2-propanol, or *tert*-butyl alcohol.

In Figure 6 the TPD curves for saturation exposures of 1-propanol, 2-propanol, and *tert*-butyl alcohol are compared. To relate the surface structure observed with STM to the reactivity of the surface, and to avoid effects due to possible changes in the surface structure due to alcohol adsorption and reaction, we performed STM on the samples prior to the runs shown in Figure 6. In all cases, the images revealed surfaces similar to those shown in Figures 3 and 4. All the alcohols tested display two desorption peaks with some unreacted alcohol plus water desorbing at 430 K, and dehydration products plus water desorbing at higher temperatures. The only reaction product observed for the primary, secondary and tertiary alcohols is the corresponding alkene. Comparing the results for 1- and 2-propanol, we see that the alkene desorption peak is 75 K higher for 1-propanol. Isobutylene formed from *tert*-butyl alcohol dehydration desorbs 140 K lower than the propene formed from the dehydration of the secondary alcohol. The peak widths of the desorbing alkenes are similar, indicating that peak shifts are dominated by changes in activation energy, rather than changes in the preexponential term. In addition, we have looked at methanol. In the same manner as the higher alcohols, some methanol desorbs unreacted at 430 K while the reaction products are observed at higher temperatures. The reaction products begin to desorb slightly below 900 K, well above the temperature observed for 1-propanol. Unfortunately, we could not fully characterize the desorption products and kinetics because heating above 900 K may irreversibly damage the WO_3 crystal.

The data show that the c(2 × 2) surface *exhibits only dehydration activity*. Since the desorption product for 1-propanol and 2-propanol is propene, the shift in propene desorption peak must mean that the desorption is reaction-rate limited. Along similar lines, despite the larger mass of isobutylene, which would be expected to lead to a higher desorption temperature than chemically similar propene, dehydration occurs at lower temperatures than the propene desorption from dehydration of the secondary alcohol.

Since water is observed to desorb at 430 K for all three alcohols, well before the alkenes are observed, deprotonation of the alcohols is fast compared to alkene formation. Therefore, the differences in alkene desorption peak temperatures as we go from primary → tertiary alcohol reflect the second step in the reaction, which is breaking the C−O bond and removing a β-hydrogen. The β-hydrogen becomes easier to remove as we go from tertiary → primary alcohol: this is the reverse of the trend we observed. Steric differences could still account for the observed alkene desorption temperatures, however this would lead to large changes in the preexponential which are not supported by the data. In contrast, C−O bonds become easier to break across the series primary → tertiary alcohol, consistent with the observed decrease in desorption peak temperature from methanol → *tert*-butyl alcohol. Therefore, C−O bond breaking must be the rate-limiting step. While this picture describes the observed trend, understanding the magnitude of the peak shifts would require greater insight into the adsorbed species' and transition state's charge distribution than is currently available in the literature.

c. STM Imaging of Alcohol Adsorption on $WO_3(001)$. To determine the active sites in the oxidative dehydration of alcohols on the $WO_3(001)$ surface, STM was performed following alcohol dosing. Attempts to image both 1-propanol and 2-propanol adsorbates immediately after dosing at room temperature failed. Under these conditions, only the c(2 × 2) periodicity of the substrate could be imaged. In this case adsorbed species would be weakly bonded to the surface, and their rapid motion in comparison with the imaging rate would render them impossible to image. This problem is regularly encountered in STM imaging of adsorbates.[42]

The simultaneous desorption of water and unreacted alcohol at 430 K suggests that the alcohols may be molecularly adsorbed at room temperature, and that heating above 400 K converts at least some of the alcohol into more strongly bound alkoxide species. Results on the adsorption of alcohols on structurally similar β-MoO_3 agree with this interpretation, since they show simultaneous water evolution and alkoxide formation, although the process occurs at room temperature.[43] To test this idea, the surface was dosed with 1-propanol at room temperature and then briefly annealed to a temperature above the water desorption peak, but below the temperature at which propene desorbs (*cf.* Figure 6). For these experiments, we chose 1-propanol because it shows the largest temperature-difference between the water and propene desorption peaks, reducing the chance of inadvertently desorbing the intermediate species. Following this procedure, new features were observed in STM images.

The $WO_3(001)$ surface in Figure 7 had been dosed with ~90 L 1-propanol (*n*-propanol) and annealed to 400 K. A distribution of bright spots that sit on the WO_3 terraces is visible, and the terraces are also discernible beneath. There is no preference for attachment at step edges or on terraces, rather the bright spots attach at defect-free terrace sites. The STM images of Figure 7a,b reveal no regular overlayer structure and similarly no evidence of an ordered overlayer was observed with

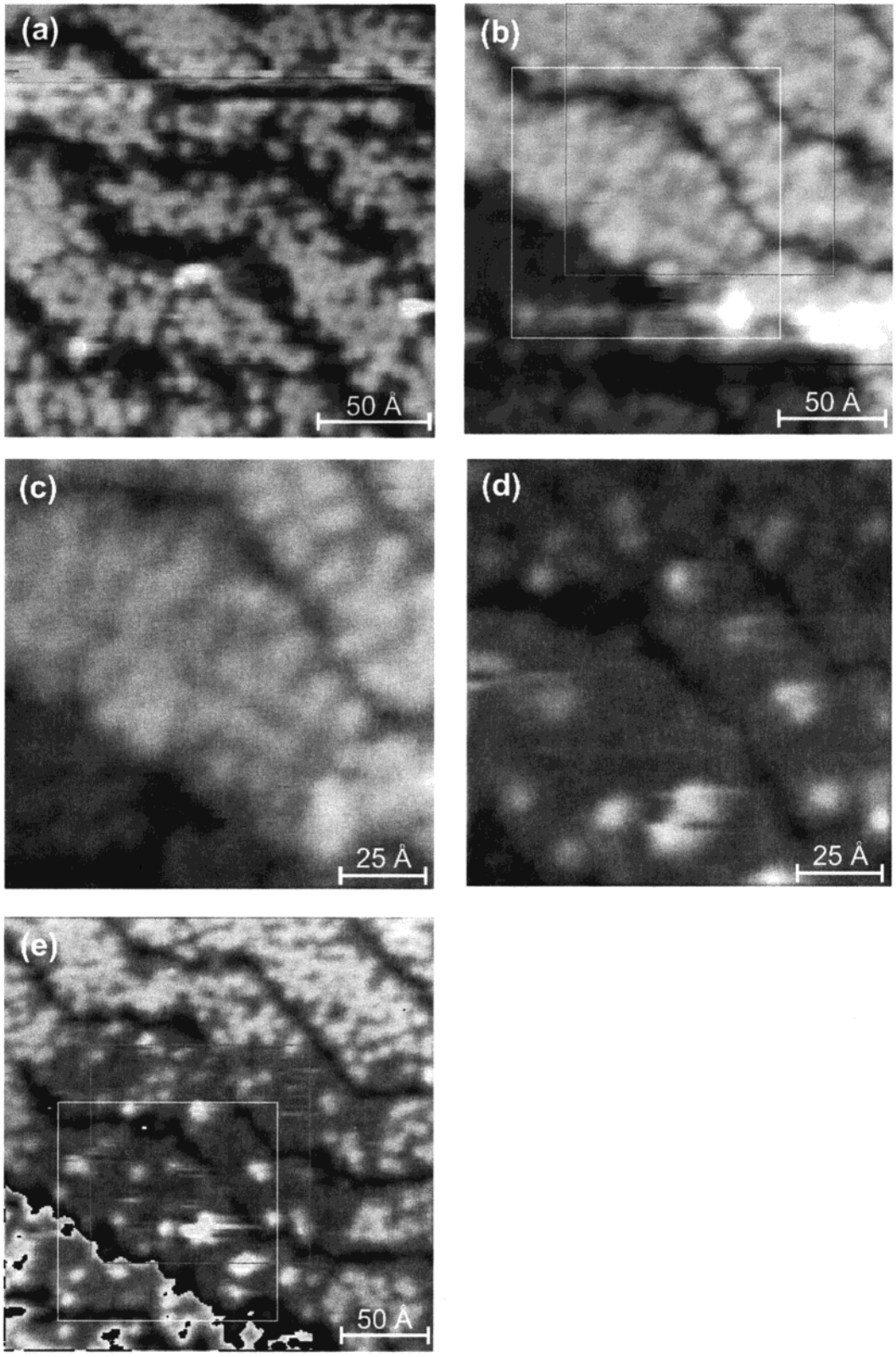

Figure 7. Images of the WO_3(001)-c(2 × 2) surface dosed with ~90 L 1-propanol and annealed to 400 K. A tunneling current of $I_t = 0.55$ nA was used throughout. (a) Wide range image at $V_B = 3.0$ V. (b) Wide range image of the surface covered with propoxide intermediates. $V_B = 2.0$ V. (c) The area represented by the white box in (b) may be re-scanned at the same bias without changing the arrangement of adsorbates ($V_B = 2.0$ V). (d) When the bias is reduced to 1.5 V, the area in the vicinity of the tip is denuded. (e) On increasing the bias and scan size, STM images show both denuded and adsorbate-covered regions. $V_B = 2.0$ V. The area in (d) is marked by a gray box in (b) and (e).

LEED. Figure 7b shows a 200 × 200 Å section of the WO_3(001) surface. The scan size was decreased to record Figure 7c. When this area was rastered for a period of several minutes, particularly at biases less than ~2.25 V, it was found that the density of bright spots diminished (Figure 7d). On increasing the scan size, an image such as that shown in Figure 7e indicates that it is the tip that has been influencing the distribution of bright features: by pushing, pulling, or picking-and-dropping, the central area in this image has been denuded of most adsorbates.

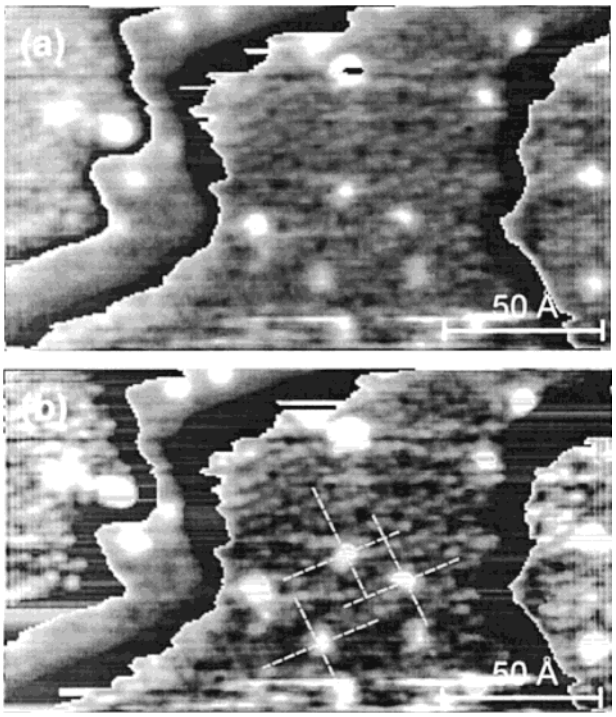

Figure 8. The c(2 × 2) surface exposed to a ~30 L dose of 1-propanol. (a) Individual alkoxide adsorbates are resolved against the atomic periodicity of the substrate, showing that they bind to exposed surface W^{6+} tungsten sites. (b) The image is repeated with enhanced contrast and guides that highlight the underlying c(2 × 2) structure. V_B = 2.5 V, I_t = 0.95 nA. To allow atomic-scale features to be seen on each of the terraces low level filtering has been applied and the contrast has been enhanced by cycling through the gray scale on each terrace.

Since water has already been evolved from surfaces heated to 400 K (Figure 6), and the alkene desorption temperature has not been reached, we assign the new bright features as bound intermediate 1-propoxide groups, that result from the dissociative adsorption of 1-propanol. The easy manipulation of the bright spots indicates that the bond with the surface is not strong, and emphasizes the need for low tunneling current and high bias to image alkoxide groups on WO_3(001) and presumably other TMO catalyst surfaces. The results also suggest a method for probing catalytic sites on oxide surfaces such as α-MoO_3 and V_2O_5 where minority defect sites are expected to be important.[12,43−46] By imaging the surface at high bias the adsorbate can be located, and then by reducing the bias the adsorbate can be swept aside, allowing the underlying site to be characterized. In the future, greater control of the adsorbate molecule may allow functionalization of the tip and a direct probe of the chemical activity of such defect sites.

As shown in Figure 8, reducing the 1-propanol exposure to ~30 L decreases the density of the bright spots attributed to 1-propoxide as expected. Analysis of Figure 7a yields a 1-propoxide coverage of 0.26 ML (1 ML = one 1-propoxide group per c(2 × 2) unit cell) while Figure 8 indicate a coverage of 0.06 ML. That the 1-propoxide coverage drops by more than a factor of 3 when the nominal exposure is reduced by a factor of 3 is most likely due to the low pumping rate of the alcohols. The alcohols tended to persist in the UHV system for quite some time after the leak valve was closed, particularly for long doses, thus leading to uncertainties in the exposure.

Figure 8 shows a surface with three different terraces, separated by single steps. The c(2 × 2) atomic periodicity of the substrate is faintly revealed simultaneously with "molecular resolution" of the adsorbed alkoxide groups. These adsorbates are attached to dark substrate lattice sites, rather than the bright features, as shown in Figure 8b where the image is repeated with enhanced contrast and guides showing the c(2 × 2) periodicity.

Since the bright features in the c(2 × 2) images correspond to terminal oxygen atoms, we are lead to the conclusion that the alkoxide groups bind to the exposed surface tungsten sites. The W^{6+} cations are coordinated to five oxygen anions and the missing oxygen ligand creates an electron deficit, making the site acidic. This Lewis acid site is then a natural choice for an approaching −OH group to bond via the O lone-pair which lowers the barrier to deprotonation to form the alkoxide, as suggested by Farneth *et al.*[43] The results directly demonstrate that this is indeed the case, and further, that once the alkoxide is bound to this site on WO_3(001)-c(2 × 2) it dehydrates to form the corresponding alkene. Similar enhanced activity at cus cations has been reported for rutile TiO_2[47] and was recently revealed on the RuO_2 surface.[48]

IV. Conclusions

Clearly the reproducibility of results from any catalytic reaction studied at the "nanoscale" depends critically on reliable surface preparation procedures. These results show that it is possible to produce WO_3(001) surfaces with a terminal oxygen coverage of 0.5 ML, and hence it is possible to control with precision the oxidation state of the surface tungsten ions. This demonstrates the suitability of the WO_3(001) surface for the investigation of catalytic reactions.

A surface that is terminated with half a monolayer of O exhibits a predominant c(2 × 2) reconstruction and readily adsorbs the alcohols methanol, 1-propanol, 2-propanol and 2-methyl-2-propanol (*tert*-butyl alcohol). Heating converts all alcohols, except methanol, to their corresponding alkenes via dehydration. No dehydrogenation products are observed desorbing from the c(2 × 2) surface. Across the series (primary → tertiary alcohol) the alkene desorption-peak temperature shifts to lower temperatures, corresponding to the lower barrier to dehydration of the alcohol. Alkene desorption is therefore reaction-rate limited, and the reaction rate is in turn limited by the rate of C−O bond scission, and not by the deprotonation rate.

STM images that visualize the atomic periodicity of the substrate simultaneously with the adsorbed alkoxide species reveal that the alkoxide groups bind to the surface W^{6+} sites exposed on the c(2 × 2) terraces, and there is no evidence that the alkoxides display any preference for the defects. The sites of this type are exposed, acidic, 5-fold coordinated W^{6+} cations. Further, we have demonstrated that it is possible to image important reactive intermediates on an oxide surface, systematically remove them with the STM tip, and then characterize the structure of the underlying adsorption site. These results powerfully demonstrate the synergistic role of the use of STM in conjunction with chemical probes to associate catalytic function with specific surface sites.

Acknowledgment. We are grateful to Russell Egdell for WO_3 samples. We thank Lana Chan and Guowen Zheng for their assistance. This work was supported by the US Department of Energy Basic Energy Sciences program, under grant DE-FG02-98ER14882.

References and Notes

(1) Salje, E. *Acta Crystallogr. B* **1977**, *33*, 574−577. The orthorhombic phase of WO_3.

(2) Madou, M. J.; Morrison, S. R. *Chemical Sensing with Solid State Devices*; Academic Press: London, 1989.

(3) Deb, S. K. *Philos. Mag.* **1973**, *27*, 801−822. Optical and photoelectric properties and color centers in thin-films of tungsten oxide.

(4) Granqvist, C. G. *Appl. Phys. A* **1993**, *57*, 19−24. Transparent conductive electrodes for electrochromic devices: a review.

(5) Gazzoli, D.; Marucci, A.; Mattei, G.; Valigi, M.; Dragone, R. *J. Phys. Chem. B* **1997**, *101*, 11129−1135. Characterization of the zirconia-supported tungsten oxide system by laser Raman and diffuse reflectance spectroscopies.

(6) Brady, R. L.; Southmayd, D.; Contescu, C.; Zhang, R.; Schwarz, J. A. *J. Catal.* **1991**, *129*, 195−201. Surface-area determination of supported oxides − WO_3/Al_2O_3.

(7) Hilbrig, F.; Gobel, H. E.; Knozinger, H.; Schmelz, H.; Lengeler, B. *J. Phys. Chem.* **1991**, *95*, 6973−6978. X-ray absorption-spectroscopy study of the titania-supported and alumina-supported tungsten-oxide system.

(8) Zhao, B.-Y.; Xu, X.-P.; Gao, J.-M.; Fu, Q.; Tang, Y.-Q. *J. Raman Spectrosc.* **1996**, *27*, 549−554. Structure characterization of WO_3/ZrO_2 catalysts by Raman spectroscopy.

(9) Kim, D. S.; Ostromecki, M.; Wachs, I. E. *J. Mol. Catal. A* **1996**, *106*, 93−102. Surface structures of supported tungsten oxide catalysts under dehydrated conditions.

(10) Barton, D. G.; Shtein, M.; Wilson, R. D.; Soled, S. L.; Iglesia, E. *J. Phys. Chem. B* **1999**, *103*, 630−640. Structure and electronic properties of solid acids based on tungsten oxide nanostructures.

(11) Burwell, R. L.; Haller, G. L.; Taylor, K. C.; Read, J. F. *Adv. Catal.* **1969**, *20*, 1−96. Chemisorptive and catalytic behavior of chromia.

(12) Friend, C. M.; Queeney, K. T.; Chen, D. A. *Appl. Surf. Sci.* **1999**, *142*, 99−105. Structure and reactivity of thin-film oxides and metals.

(13) Hermann, K.; Witko, M.; Druzinic, R. *Faraday Discuss.* **1999**, *114*, 53−66. Electronic properties, structure and adsorption at vanadium oxide: density functional theory studies.

(14) Woodward, P. M.; Sleight, A. W.; Vogt, T. *J. Solid State Chem.* **1997**, *131*, 9−17. Ferroelectric tungsten trioxide.

(15) Diehl, R.; Brandt, G.; Salje, E. *Acta Crystallogr. B* **1978**, *24*, 1105−1111. The crystal structure of triclinic WO_3.

(16) Locherer, K. R.; Swainson, I. P.; Salje, E. K. H. *J. Phys.: Condens Matter* **1999**, *11*, 4143−4156. Transition to a new tetragonal stage of WO_3: crystal structure and distortion parameters.

(17) Loopstra, B. O.; Boldrini, P. *Acta Crystallogr.* **1966**, *21*, 158−162. Neutron diffraction investigation of WO_3.

(18) Rosen, C.; Banks, E.; Post, B. *Acta Crystallogr.* **1956**, *9*, 475. The thermal expansion and phase transitions of WO_3.

(19) Salje, E. *Acta Crystallogr. B* **1974**, *7*, 615−617. A new type of electrooptic effect in semiconducting WO_3.

(20) Sundberg, M. *J. Solid State Chem.* **1980**, *35*, 120−127. Structure and oxidation behavior of $W_{24}O_{70}$, a new member of the (103) CS series of tungsten oxides.

(21) Tasker, P. W. *J. Phys. C: Solid State Phys.* **1979**, *12*, 4977−4984. The stability of ionic crystal surfaces.

(22) Jones, F. H.; Rawlings, K.; Foord, J. S.; Cox, P. A.; Egdell, R. G.; Pethica, J. B.; Wanklyn, B. M. R. *Phys. Rev. B* **1995**, *52*, R14392−R14395 [Corrected: *Phys. Rev. B* **1996**, *53*, 10412]. Superstructures and defect structures revealed by atomic-scale STM imaging of WO_3(001).

(23) Jones, F. H.; Rawlings, K.; Foord, J. S.; Egdell, R. G.; Pethica, J. B.; Wanklyn, B. M. R.; Parker, S. C.; Oliver, P. M. *Surf. Sci.* **1996**, *359*, 107−121. An STM study of surface structures on WO_3(001).

(24) Jones, F. H.; Dixon, R. A.; Brown, A. *Surf. Sci.* **1996**, *369*, 343−350. Observation of reduced (1 × 1) terraces on WO_3(001) surface using scanning tunnelling microscopy.

(25) Dixon, R. A.; Williams, J. J.; Morris, D.; Rebane, J.; Jones, F. H.; Egdell, R. G.; Downes, S. W. *Surf. Sci.* **1998**, *399*, 199−211. Electronic states at oxygen deficient WO_3(001) surfaces: a study by resonant photoemission.

(26) Stachiotti, M. G.; Corà, F.; Catlow, C. R. A.; Rodriguez, C. O. *Phys. Rev. B* **1997**, *55*, 7508−7514. First-principles investigation of ReO_3 and related oxides.

(27) Corà, F.; Patel, A.; Harrison, N. M.; Dovesi, R.; Catlow, C. R. A. *J. Am. Chem. Soc.* **1996**, *118*, 12174−12182. An ab initio Hartree−Fock study of the cubic and tetragonal phases of bulk tungsten trioxide.

(28) Corà, F.; Stachiotti, M. G.; Catlow, C. R. A.; Rodriguez, C. O. *J. Phys Chem. B* **1997**, *101*, 3945−3952. Transition metal oxide chemistry: electronic structure study of WO_3, ReO_3 and $NaWO_3$.

(29) Corà, F.; Catlow, C. R. A. *Faraday Discuss.* **1999**, *114*, 421−442. QM investigations on perovskite-structured transition metal oxides: bulk, surfaces and interfaces.

(30) Oliver, P. M.; Parker, S. C.; Egdell, R. G.; Jones, F. H. *J. Chem. Soc., Faraday Trans.* **1996**, *92*, 2049−2056. Computer simulation of the surface structures of WO_3.

(31) Bullett, D. W. *J. Phys. C* **1983**, *16*, 2197−2207. Bulk and surface electron states in WO_3 and tungsten bronzes.

(32) Langell, M. A.; Bernasek, S. L. *J. Vac. Sci. Technol.* **1980**, *17*, 1296−1302. Transition metal compound surfaces II: the tungsten trioxide single-crystal surface.

(33) Bringans, R. D.; Höchst, H.; Shanks, H. R. *Phys. Rev. B* **1981**, *24*, 3481−3489. Defect states in WO_3 studied with photoelectron spectroscopy.

(34) Salje, E.; Carley, A. F.; Roberts, M. W. *J. Solid State Chem.* **1979**, *29*, 237−251. The effect of reduction and temperature on the electronic core levels of tungsten and molybdenum in WO_3 and $W_xMo_{1-x}O_3$ − a photoelectron spectroscopy study.

(35) De Angelis, B. A. Schiavello, M. *J. Solid State Chem.* **1977**, *21*, 67−72. X-ray photoelectron spectroscopy study of nonstoichiometric tungsten oxides.

(36) Nakakura, C. Y.; Phanse, V. M.; Zheng, G.; Bannon, G.; Altman, E. I.; Lee, K. P. *Rev. Sci. Instrum.* **1998**, *69*, 3251−3258. A high-speed, variable-temperature, ultrahigh vacuum scanning tunneling microscope.

(37) Zheng, G.; Altman, E. I. *Surf. Sci.* **2000**, *462*, 151−168. The oxidation of Pd(111).

(38) Wanklyn, B. M.; Garrard, B. J. *J. Mater. Sci. Lett.* **1983**, *2*, 285−290. The flux growth of some simple and complex oxides.

(39) Tanner, R. E.; Castell, M. R.; Briggs, G. A. D. *Surf. Sci.* **1998**, *412−413*, 672−681. High-resolution scanning tunnelling microscopy of the rutile TiO_2(110) surface.

(40) Tanner, R. E.; Meethunkij, P.; Altman, E. I. *J. Vac. Sci. Technol. A*, submitted.

(41) Smith, R. L.; Rohrer, G. S. *J. Catal.* **1998**, *173*, 219−228. The protonation of MoO_3 during the partial oxidation of alcohols.

(42) Chiang, S. In *Scanning Tunneling Microscopy I*; Güntherodt, Wiesendanger, R., Eds.; Springer-Verlag: Berlin, 1992.

(43) Farneth, W. E.; McCarron, E. M.; Sleight, A. W.; Staley, R. H. *Langmuir* **1987**, *3*, 217−223. Comparison of the surface-chemistry of 2 polymorphic forms of molybdenum trioxide.

(44) Chowdhry, U.; Ferretti, A.; Firment, L. E.; Machiels, C. J.; Ohuchi, F.; Sleight, A. W.; Staley, R. H. *Appl. Surf. Sci.* **1984**, *19*, 360−372. Mechanism and surface structural effects in methanol oxidation over molybdates.

(45) Ohuchi, F.; Firment, L. E.; Chowdhry, U.; Ferretti, A. *J. Vac. Sci. Technol. A* **1984**, *2*, 1022−1023. Adsorption and temperature-programmed desorption of methanol on MoO_3 powder and crystal surfaces.

(46) Lewis, K. B.; Oyama, S. T.; Somorjai, G. A. *Appl. Surf. Sci.* **1991**, *52*, 241−248. TPD studies of vanadium-oxide films deposited on gold.

(47) Onishi, H.; Iwasawa, Y. *Chem. Phys. Lett.* **1994**, *226*, 111−114. STM imaging of formate intermediates adsorbed on a TiO_2(110) surface.

(48) Over, H.; Kim, Y. D.; Seitsonen, A. P.; Wendt, S.; Lundgren, E.; Schmid, M.; Varga, P.; Morgante, A.; Ertl, G. *Science* **2000**, *287*, 1474−1476. Atomic-scale structure and catalytic reactivity of the RuO_2(110) surface.